Solution Structures of Antimalarial Drug−Heme Complexes†

Alison Leed,‡,§ Kateri DuBay,‡ Lyann M. B. Ursos, Devin Sears,‖ Angel C. de Dios, and Paul D. Roepe*

Department of Chemistry, Department of Biochemistry and Molecular Biology, and Program in Tumor Biology, Lombardi Cancer Center, Georgetown University, 37th and O Streets, Washington, D.C. 20057

Received March 12, 2002; Revised Manuscript Received May 31, 2002

ABSTRACT: Paramagnetic metal centers [such as Fe^{III} found within ferriprotoporphyrin IX heme (FPIX)] exert through space effects on the relaxation rate of nearby proton spins that depend critically on the metal−proton distance. We have measured these effects for all protons of several antimalarial drugs that bind to FPIX by systematically varying the drug:heme molar ratio in high field NMR experiments. These measurements allow us to determine precise FPIX Fe−drug H distances for the solution structures of noncovalent complexes formed between FPIX μ-oxo dimers and the antimalarial drugs chloroquine (CQ), quinine (QN), and quinidine (QD). Using these distances, we then performed distance restraint calculations to determine the lowest-energy solution structures of these complexes. Structures were solved for neutral, monoprotic (+1), and diprotic (+2) forms of the drugs. Analysis of these structures allows us to visualize for the first time the stereospecific differences between QN and QD binding to FPIX and the differences in populations of QN and QD solution structures upon changes in digestive vacuolar pH for drug resistant malarial parasites [Dzekunov, S. M., et al. (2000) *Mol. Biochem. Parasitol. 110*, 107−124]. The data indicate a previously unrecognized key role for the CQ aliphatic chain in stabilizing FPIX−CQ complexes, and suggest how lengthening or shortening the chain might perturb stability. We also define FPIX:drug stoichiometries of 2:1 for the complexes formed at physiological FPIX concentrations, in contrast to the 4:1 and 5:1 stoichiometries previously determined at higher FPIX concentrations [Dorn, A., et al. (1998) *Biochem. Pharmacol. 55*, 727−736]. These atomic resolution antimalarial drug−heme structures should help elucidate how these drugs inhibit formation of hemozoin during metabolism of heme within the malarial parasite *Plasmodium falciparum* and assist ongoing development of strategies for circumventing antimalarial drug resistance.

The mechanisms of action of key antimalarial drugs such as the 4-aminoquinoline derivative chloroquine (CQ)[1] are not completely understood. Additional molecular level data are sorely needed to better understand this pharmacology, and hence the molecular pathways to CQ resistance (CQR) in *Plasmodium falciparum* malarial parasites. CQR malaria is a leading and rapidly growing cause of death in many countries. A principle mode of action of CQ and related quinoline drugs is inhibition of hemozoin formation within the lysosomesque "digestive vacuole" (DV) of the parasite. Hemozoin is the optically dense "malaria pigment" that appears as a dark black spot in the red blood cells (RBCs) of infected patients. It is a chemically fascinating detoxified form of ferriprotoporphyrin IX (FPIX) heme that appears to be an Fe−O41 reciprocal dimer crystal (*1*). It is derived ultimately from free FPIX released along with superoxide upon digestion of nutritious red cell hemoglobin within the DV.

Inhibition of hemozoin formation by antimalarial drugs is believed to be via the high affinity they have for one or more of the various possible chemical forms of monomeric or dimeric FPIX that are likely found in the parasite DV (*2*, *3*). Again, crystallized hemozoin is nontoxic to malarial parasites, but large amounts of free monomeric or dimeric heme (and/or their drug conjugates) are toxic. It is possible that multiple drug−heme binding events are relevant for antimalarial pharmacology, since at least three forms of heme likely exist as hemozoin precursors (namely, the FPIX aqua monomer, the μ-oxo dimer, and the Fe−O41 dimer). Moreover, since the low pH and high Cl concentration likely present in the DV could conceivably catalyze Markovnikov addition at vinyl side chains of FPIX, these three forms might also exist as the progeny of chemically modified FPIX. In the elucidation of the details of antimalarial pharmacology as well as the mechanisms of resistance to antimalarial drugs, determining the biological lifetimes of these possible forms of FPIX and the structures of the variety of possible drug−FPIX complexes is essential. Nitrogen donor ligands can readily form covalent complexes with the Fe centers of porphyrins (*4*, *5*). Thus, not surprisingly, it has been proposed that various nitrogen-containing antimalarial drugs (i.e., CQ, QN, and QD) might form covalent complexes with monomeric FPIX via an Fe−N bond, assuming the monomeric

† This work was supported by grants from the NIH (AI45957) and the Burroughs Wellcome Foundation to P.D.R., and an NSF career award to A.C.d.D.

* To whom correspondence should be addressed. Telephone: (202) 687-7300. Fax: (202) 687-6209. E-mail: roepep@gusun.georgetown.edu.

‡ These authors contributed equally to this research.

§ Current address: Department of Biological Chemistry and Molecular Pharmacology, Harvard Medical School, Boston, MA 02115.

‖ Current address: Department of Chemistry, University of Illinois at Chicago, Chicago, IL 60607.

[1] Abbreviations: CQ, chloroquine; CQR, chloroquine resistance (resistant); DV, digestive vacuole; RBC, red blood cell; FPIX, ferriprotoporphyrin IX; QN, quinine; QD, quinidine; SD, standard deviation.

10.1021/bi020195i CCC: $22.00
Published on Web 07/18/2002

species can be stabilized in the DV as is the case in some organic solvents.

However, in aqueous solution, the μ-oxo dimer form of FPIX dominates, wherein O (from H_2O) bridges two monomers via a nearly linear Fe−O−Fe bond. A general picture of FPIX μ-oxo dimer−quinolinal drug complexes has emerged from early one-dimensional (1D) NMR studies. These models were based on analysis of how the paramagnetic Fe^{III} center of FPIX broadened aromatic versus aliphatic proton (*6*, *7*) or carbon (*8*, *9*) resonances of CQ and quinine (QN). These important data suggested that noncovalent $\pi-\pi$ interactions between the heme tetrapyrrole and drug quinolinal rings were likely quite significant in determining the stability of drug−heme complexes, and that the interplanar distance between the heme and drug was between 3 and 5 Å (*7*). However, in these studies, it was not possible to map exact atomic level distances between the drug and μ-oxo dimer heme. Thus, differences in the geometry of complexes that exist for chemically related antimalarials that nonetheless have different activities (i.e., QN vs QD) are currently unknown. In addition, differences in these structures for various protonated species of weakly dibasic drugs are unknown.

Since mutation of the antimalarial drug target (again, DV heme released upon digestion of RBC hemoglobin) is outside the genetic control of the parasite, chemical or physiological events that even subtly alter the efficiency of drug−heme binding are predicted to be a principle cause of antimalarial drug resistance (*10*−*12*). Since antimalarials are in general amphipathic monoprotic or diprotic weak bases, and since monomeric FPIX is an amphipathic diprotic weak acid, one might guess that conditions which influence the interaction between such species (e.g., pH, ionic strength, etc.) should be central in determining precise drug−heme complex geometries. This idea is further supported by recent evidence that supports DV pH (*10*, *13*, *14*) and salt (*15*) changes in CQR parasites.

For these reasons, we have used paramagnetic relaxation effects to determine precise distance constraints for the solution structures formed between FPIX μ-oxo dimers and three aminoquinolinal antimalarial drugs (CQ, QN, and QD) at several pHs. Using these distance constraints and XPLOR energy minimization, we deduce the first solution structures of antimalarial drug−heme complexes at atomic resolution.

MATERIALS AND METHODS

Materials. Ferriprotoporphyrin IX hydroxide (FPIX), chloroquine diphosphate salt (CQ), quinidine gluconate, and quinidine hydrochloride monohydrate (QD) were purchased from Sigma (St. Louis, MO). Quinine dihydrochloride (QN) was from BDH Chemicals Ltd (Poole, England). Deuterium oxide was from Cambridge Isotope Laboratory (Andover, MA). NMR tubes (5 mm) were purchased from Wilmad Glass Co., Inc. (Buena, NJ). All other reagents were analytical grade or better and were used without additional purification.

Sample Preparation. Stock solutions (20 mM) of the individual antimalarial drugs (CQ, QD, and QN) were made in D_2O. A 20 mM FPIX stock solution was made in dilute NaOH in D_2O. Under these conditions, FPIX exists primarily as a μ-oxo dimer, where the bridging oxygen is donated from a heavy water molecule. Different drug/FPIX dimer mixtures were prepared in 1.5 mL microcentrifuge tubes with a total volume of 1 mL, and these mixtures were then transferred into 5 mm NMR tubes. To measure paramagnetic relaxation effects, an increasing amount of FPIX (final concentrations ranging from 0 to 1.0 mM) was added to 10 mM drug in 1.5 mL microcentrifuge tubes, and D_2O was used to adjust the sample volume to 1 mL.

NMR Spectroscopy. All experimental data were collected on a Varian Unity Inova 500 MHz spectrometer using the Varian VNMR version 5.1 software. Sample and instrument temperatures were controlled at 298 K. For drug proton peak assignments, 1D proton NMR and double-quantum COSY experiments were performed on 10 mM drug samples without FPIX. Importantly, at FPIX:drug ratios where clear assignments of drug protons are possible, we did not observe changes in drug chemical shifts when the FPIX:drug ratio was increased.

Proton longitudinal relaxation times (T_1 values) were measured using a standard inversion recovery pulse sequence while presaturating any residual water peak. T_1 values were measured for free drug samples (10 mM) in the absence of FPIX, and for drug/FPIX dimer solutions at increasing concentrations of FPIX dimer, but at a constant drug concentration. At increasing FPIX dimer:drug ratios, more drug is complexed with FPIX dimer at any given instant, leading to increasingly larger effects on T_1 due to the paramagnetic FPIX Fe (see the Results). These data were then converted to effective relaxation rates (R):

$$R(\text{observed}) = 1/T_1(\text{observed}) = (1 - f)R(\text{complex}) + fR(\text{free}) \quad (1)$$

where R(complex) is the relaxation rate for the drug fully bound to FPIX dimer, R(free) is the relaxation rate of the free drug, and f is the mole fraction of free drug. Also

$$R(\text{observed}) = [R(\text{complex}) - R(\text{free})][E_0/(K_D + S_0)] + R(\text{free}) \quad (2)$$

where E_0, S_0, and K_D are the concentrations of FPIX dimer and antimalarial drug and the relevant dissociation constant, respectively. Initial values for K_D were taken from the literature (*17*), and QN K_D values were used as initial estimates for QD K_D. We note that measured T_1 values correspond to the reciprocal of observed line widths at the same FPIX:drug ratio (data not shown), meaning that T_1 decreases at the same rate that the corresponding line width increases. Thus, very short correlation times for the drug−FPIX dimer complexes are relevant for our analysis.

In using these expressions, we make the following assumptions. (1) FPIX is predominantly in the μ-oxo dimer form. (2) The association constant for the drug and μ-oxo dimer is large. (3) Due to the linearity of R versus [drug]:[FPIX dimer] ratio plots, the stoichiometry between drug and μ-oxo dimer is 1:1 at these concentrations (see the Results). (4) At the drug:FPIX dimer ratios used in this study, very little free μ-oxo dimer is present at equilibrium since the drug is always in large excess and K_A is large.

Values of R(observed) versus FPIX dimer concentration were plotted so that R(complex) could be calculated from the slope to the straight line fit (see the Results). These R

values were then converted to Fe−drug proton distances using the Solomon−Bloembergen equation as described in Determination of Distance Constraints below.

Determination of the Fe Spin State. To use the Solomon−Bloembergen equation, the heme Fe spin state must be known. We used the Evans method (*18*) to measure the Fe spin state for either free μ-oxo dimer or dimer in the presence of equimolar CQ under conditions that mimicked those for the inversion recovery measurements. Reference reporter protons were from 3% tBuOH dissolved in the FPIX dimer or dimer/drug solutions as described previously (*18*). We observed shifts of −0.204 and −0.198 ppm in the absence and presence of equimolar CQ, respectively (not shown). After adjusting for minor monomeric FPIX (spin = $^5/_2$Fe) present in the samples, we calculated a spin of $^1/_2$ for μ-oxo dimer Fe in either the absence or presence of CQ (*18*).

Determination of Distance Constraints. Relaxation rates of individual protons were converted into distances to the paramagnetic Fe center at one face of the μ-oxo dimer by applying the Solomon−Bloembergen equation:

$$R(\text{complex}) = \left(\frac{\mu_0}{4\tau}\right)^2 \frac{(\gamma_N^2 g_e^2 \mu_b^2)(S+1)}{r^6} \tau_c \qquad (3)$$

where S is the total electron spin, r is the distance between the proton and the paramagnetic Fe, and γ_N, g_e, μ_0, and μ_b are constants. The effective correlation time (τ_c–) is defined via the relation $1/\tau$(effective) = $1/\tau$(rotation) + $1/\tau$(exchange) + $1/\tau$(electron relaxation). It is essentially equal to τ(electron relaxation) [2×10^{-12} s (20)] for the following reasons. (1) The rotational correlation time of the large FPIX dimer−drug complex will be on the order of 10^{-8}−10^{-9} s. (2) The exchange correlation time is not diffusion-limited since there is measurable binding energy and exchange occurs on a time scale of $>10^{-8}$ s. (3) We may neglect rotational and exchange contributions if the electron relaxation time is orders of magnitude shorter, as in this case.

The determined proton−Fe distances were then used as distance restraints in ab initio molecular dynamics calculations using X-PLOR software.

Molecular Modeling. Force field parameters for the three different antimalarial drugs were calculated on a cluster of workstations at the University of Illinois at Chicago (Chicago, IL) using Gaussian98 software to minimize structures formed using InsightII software (Accelrys, San Diego, CA). Force field parameters for FPIX μ-oxo dimer were modified from an FPIX force field kindly provided by M. McMahon (Department of Chemistry, Massachusetts Institute of Technology, Cambridge, MA). All of the resulting parameters were combined, and drug structures were energy minimized together with that of the FPIX dimer. Initial templates for the drug−FPIX dimer complexes were constructed using the Gaussian preminimized structures and stereospecific dihedral angles. The templates then underwent full structure distance geometry embedding calculations (nmr/dg_full_embed.inp), followed by a distance geometry/simulated annealing protocol (nmr/dgsa.inp). This step (dgsa) involved cooling from an initial temperature of 2000 K, with 100 000 total steps involved in "cooling" the structures. This process was subject to planarity restraints and program-derived geometric constraints, as well as the experimentally determined proton−Fe distance restraints described above. The resulting three-dimensional structures were then subjected to a simulated annealing refinement using the X-PLOR nmr/refine.inp protocol. In this step, the structures were subjected to the same planarity, geometric, and distance constraints, as well as electrostatic restraints from the force field parameters. Refinement began with an initial annealing temperature of 1000 K, and structures were allowed to cool in a total of 200 000 steps. Final models were viewed within InsightII using the atomic coordinates of the energy-minimized structures. Models with unrealistically high energies due to bonding or planarity violations were discarded. Models with valid energies were placed into groups with overlapping solutions, and those that best fit the experimentally determined distance constraints provided by NMR (all proton−Fe distances within ±1.00 Å of that measured) are used in the Results to display and discuss key trends for these structures.

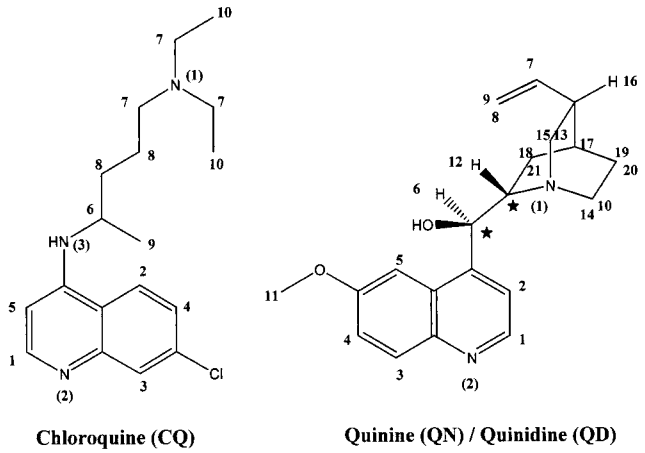

FIGURE 1: Structures of CQ (left) and QN and QD (right). The two chiral carbons that differ between QN (*S*,*R*) and QD (*R*,*S*) are labeled with stars. Protons are labeled on the basis of the position of the relevant peaks in the NMR spectra (see Figure 2A below), and this proton labeling scheme is also used in Figure 3 and Tables 1−3, which give drug H−FPIX Fe distances after XPLOR energy minimization (see the text). When more than one copy of a numeral appears, it indicates the protons are chemically equivalent (hence, NMR peaks overlap). Note we do not distinguish individual protons for methyl groups; hence, the distance constraints calculated for these (see the text) represent the average for all three. N atoms are also numbered (in parentheses) for reference.

Analysis of Reported Structures. We have made the following reasonable assumptions in this work. (1) The observed longitudinal relaxation rate is attributed solely to a dipolar mechanism. (2) Only a single stoichiometric complex species is in equilibrium with the free drug, and the drug−dimer complex stoichiometry is 1:1 (see the Results). (3) Only a single geometric isomer of this complex species is present, and its geometry will be obtained by applying all measured distance constraints. Because of the absence of contact shifts (see above) and the very good fit we obtain for 1:1 stoichiometry (see the Results), the first two assumptions are valid. However, the third assumption cannot be absolutely proven by the experiments presented here. The interaction between the drug and FPIX dimer is likely dynamic, and the R that we measure could be time averaged over several structures. Nonetheless, although the energy-minimized structures we present may not be the only

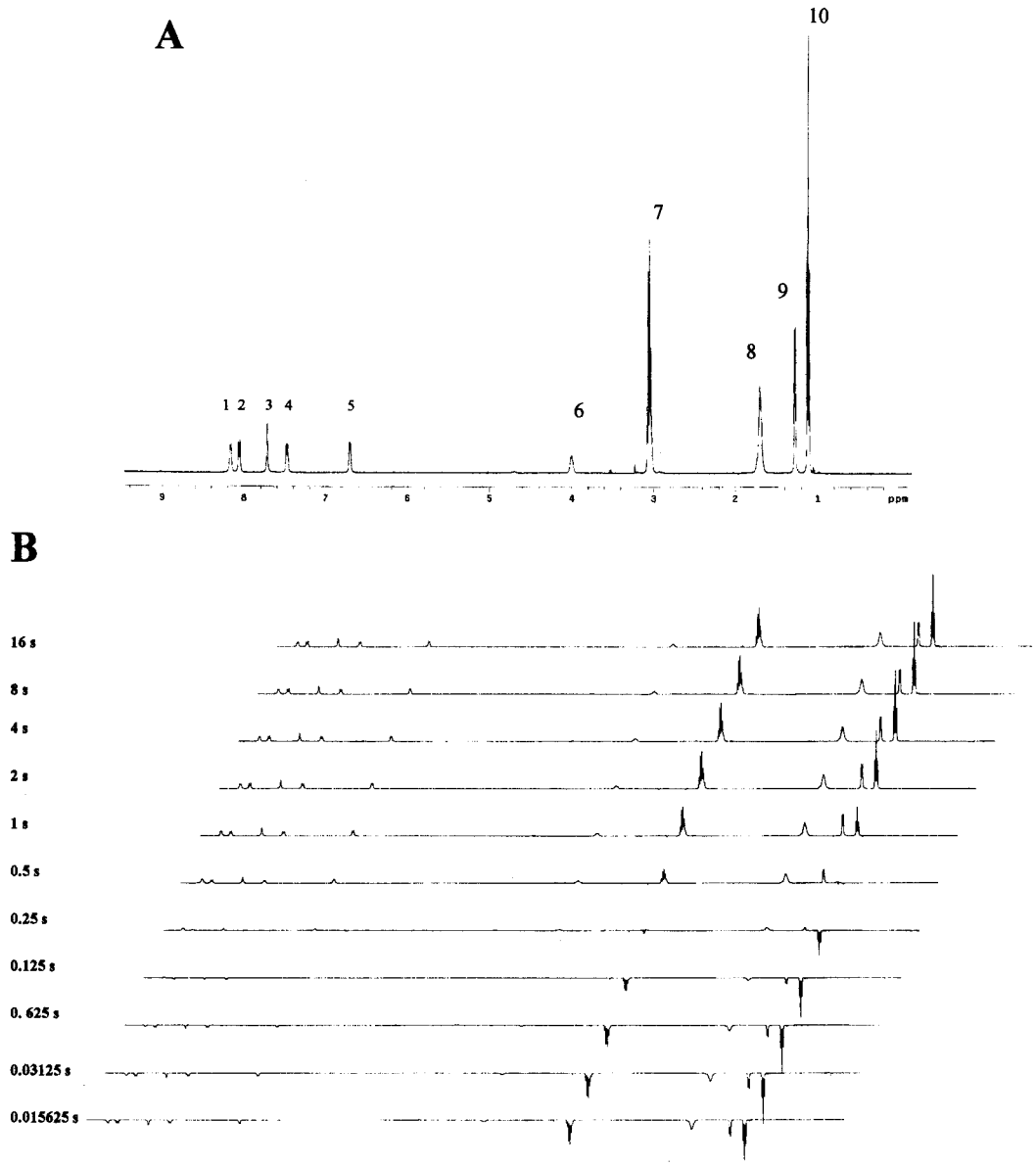

FIGURE 2: (A) 1D NMR spectrum of 10 mM CQ at pH 6.5. Peak assignments are consistent with previous work (*6*, *7*, *21*) and are denoted in Figure 1 (left). (B) Example of an inversion recovery experiment for a 100:1 CQ/FPIX mixture (the top spectrum is identical to the 1D spectrum shown in panel A). Similar data are obtained at other CQ:FPIX ratios, but null points for the H resonances (see the text) are of course altered as an increasing amount of paramagnetic Fe is titrated into the solution.

solutions formally compatible with the measured distance constraints, the averaged structures we present provide considerable new insight that is consistent with the experimental data.

RESULTS

NMR-Derived Distance Constraints. Figure 1 presents the structures of the antimalarial drugs used in this work and the numbering scheme for individual drug protons. Figure 2A presents the one-dimensional NMR spectrum of 10 mM CQ at pH 6.5. Peak assignments to individual CQ protons (see Figure 1) are straightforward and consistent with previous NMR analysis (*6*, *21*). Figure 2B presents representative T_1 experimental data. In this example, CQ and FPIX dimer were mixed at a 100:1 molar ratio. As shown, specific CQ protons "relax" with a characteristic half-time that is in part due to the fluctuating magnetic field provided by the unpaired electron on the Fe atom of FPIX. For example, note aliphatic CQ protons labeled 10 in Figure 1 (to the far right, Figure 2B) recover with a characteristic null time (T_1/0.693) near 0.5 s, whereas aromatic CQ protons (labeled 1−5 in Figure 1 and to the far left, Figure 2B) recover more quickly (approximately 0.13 s) as expected on the basis of their proximity to the unpaired electron. Increasing the FPIX:CQ ratio in the NMR tube (see Materials and Methods) decreases the recovery time for all CQ protons (Figure 3). Importantly, as shown in Figure 3, plots of $1/T_1$ versus FPIX:CQ ratios have steep slopes, indicating strong Fe paramagnetic effects, and the line shapes are linear, not quadratic, indicating a stoichiometry of one drug molecule per one FPIX dimer in the solution complex. Previously, a stoichiometry of one drug per two dimers (four FPIX tetrapyrroles) was suggested for the CQ−FPIX complex, based on line broadening in NMR spectra of CQ/FPIX mixtures (*6*). Although estimates of stoichiometry that come from line broadening effects are less quantitative than those calculated in the work presented here,

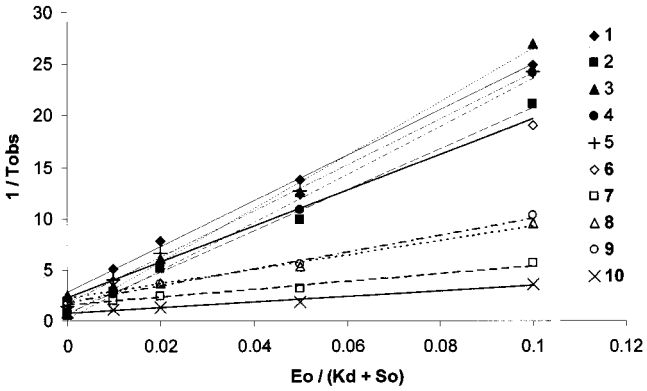

FIGURE 3: Plot of $1/T_{observed}$ vs [FPIX] $(E_0)/[K_d(17) + [CQ]S_0]$ for CQ protons (cf. Figure 1 for the proton labeling scheme). [CQ] is constant (see Materials and Methods), but [FPIX] is increased in the series of NMR experiments, providing increasing paramagnetic effects on observed longitudinal relaxation for individual protons (Figure 2). From plots such as these, $1/T_1$ values for drug bound to FPIX are easily determined (see Materials and Methods) and are then used to compute explicit CQ H−FPIX Fe distances (see Materials and Methods).

importantly, another study that used scanning calorimetry to investigate stoichiometry also suggested 1:4 (CQ:FPIX) stoichiometry (*17*). This estimate may have been influenced by the higher FPIX concentration used in the analysis and/or the solid state nature of some samples, since, in contrast, another recent study determined 1:1 stoichiometry in 40% aqueous DMSO solutions (*22*). Regardless, our results (at these CQ:FPIX ratios in a physiological solution) are quite clear: if a stoichiometry of 1:4 (CQ:FPIX) were indeed the case for these samples, plots such as those in Figure 3 would not be linear but would present a characteristic hyperbolic shape. We note that in all analyses that follow (CQ, QN, and QD at several pHs) such $1/T_1$ versus E_0/S_0 plots were distinctly linear for all protons, indicating one drug per FPIX dimer stoichiometries for the solution complexes at these ratios and under these conditions.

As described in Materials and Methods, plots such as those shown in Figure 3, along with application of the Solomon−Bloembergen equation, provide explicit distances between FPIX Fe and individual drug protons. Table 1 presents such distances for the complexes formed between either neutral, monoprotic (+1), or diprotic (+2) CQ and FPIX μ-oxo dimers in solution, after optimization via XPLOR as described below (note distances before and after application of XPLOR are essentially the same; data not shown). Distances for the different CQ species were obtained by manipulating the pH in the NMR experiment (see Materials and Methods) and were refined with XPLOR (see below). We observe significant changes in many of the Fe−H distances upon changing between neutral, +1, and +2 CQ species, indicating rearrangement of the drug−FPIX dimer complex upon protonation of the aliphatic (N1) and quinolinal aromatic (N2) nitrogens (cf. Figure 1). Similar magnitude pH-dependent Fe−H distance changes were found for QN and QD (Tables 2 and 3). These are dicussed below in Atomic Level Geometries of the Complexes in the Results.

Energies of the Drug−FPIX Complex Structures. With these experimentally determined Fe−H distances in hand, XPLOR calculations (*23*−*25*) were then performed to determine energetically favorable complex geometries. Note XPLOR solutions for these noncovalent complexes are only possible with the distance constraints in hand, and that these constraints provide a unique set of energetically reasonable solutions. From each energy minimization, a set of 30 solutions that satisfied the distance constraints were obtained, and the energies and drug−heme complex geometries were tabulated. In each of the nine possible cases (CQ, QN, and QD; neutral vs +1 vs +2 for each), a small subset of three to eight solutions was found that satisfied all experimentally determined distance constraints less than or equal to ±1.0 Å. Not coincidentally, these are also the lowest-energy (most stable) solutions as defined by XPLOR. The atomic level geometries of these complexes are discussed in the next section. The energies for the set of all valid solutions (valid meaning only that they do not violate symmetry, bond lengths, bond angles, etc.), which includes some solutions with distance constraint violations as high as ±1.5 Å, are shown in Figure 4. Note that energy comparisons among complexes formed with different drug species (e.g., neutral, monoprotic, and diprotic QN) or comparisons between complexes for similarly protonated QN and QD isomers depend on XPLOR calculations that use very similar drug force field functions, so these comparisons are indeed valid. However, comparisons between (for example) monoprotic CQ and monoprotic QN are merely semiquantitative since the relevant XPLOR calculations use different drug force fields. Regardless, inspection of the trends in these plots offers several simple yet important conclusions.

First, energies for the monoprotic QN−FPIX complex are lower than those of the monoprotic QD−FPIX complex, suggesting a higher heme affinity for QN than for QD in

Table 1: Chloroquine H− and N−Fe Distances[a]

	neutral		monoprotic (+1)		diprotic (+2)	
atom	±1.00 Å	SD	±1.00 Å	SD	±1.00 Å	SD
H1	4.569	0.313	4.445	0.304	4.515	0.205
H2	3.845	0.483	3.633	0.449	3.383	0.349
H3	4.757	0.069	4.687	0.060	4.726	0.048
H4	4.914	0.078	4.696	0.106	4.687	0.077
H5	4.037	0.747	3.827	0.732	3.676	0.453
H6	3.651	0.564	3.492	0.639	3.950	0.657
H7a	5.872	0.633	5.441	0.731	5.731	0.441
H7b	5.987	0.605	5.132	0.723	5.830	0.148
H7c	5.356	0.884	5.114	0.852	5.058	0.791
H7d	5.115	0.760	4.820	0.872	5.332	0.711
H7e	5.344	0.734	5.214	0.866	5.210	0.932
H7f	5.615	0.807	4.958	0.829	4.874	0.655
H8a	5.501	0.352	5.394	0.249	5.463	0.036
H8b	5.803	0.031	5.152	0.443	5.318	0.306
H8c	4.805	0.813	4.609	0.863	4.321	0.929
H8d	4.787	1.006	4.269	0.890	4.540	0.829
H9a−c	5.088	0.581	4.919	0.515	4.842	0.522
H10a−c	6.038	0.714	5.774	0.645	5.710	0.655
H10d−f	6.052	0.621	5.775	0.655	5.799	0.632
N3	3.447	0.903	3.137	0.872	2.759	0.568
N1	4.744	0.353	5.260	0.240	4.559	0.420
N1H			6.134	0.703	3.983	1.231
N2	3.951	0.234	3.938	0.239	3.965	0.157
N2H					4.607	0.228

[a] Mean FPIX Fe−drug H distances (in angstroms) for complexes formed with neutral, +1, and +2 CQ. These values are the initial distances from NMR T_1 experiments, followed by XPLOR refinement as described. The final values from all valid XPLOR output solutions were averaged to compute the mean, which (in each case) is within 1 Å of the initial NMR experimental value.

Table 2: Quinine H− and N−Fe Distances[a]

	neutral		monoprotic (+1)		diprotic (+2)	
atom	±1.50 Å	SD	±1.00 Å	SD	±1.00 Å	SD
H1	5.392	0.023	6.854	0.012	5.924	0.007
H2	5.109	0.251	6.065	0.023	5.256	0.022
H3	5.078	0.043	6.770	0.026	5.837	0.019
H4	5.095	0.016	6.771	0.059	5.823	0.049
H5	4.187	0.731	4.914	0.031	4.258	0.025
H6	4.553	1.043	4.758	0.585	4.387	0.754
H7	5.613	0.636	7.820	0.451	6.870	0.429
H8	5.762	0.107	7.182	0.127	6.246	0.047
H9	5.691	0.263	8.161	0.504	7.012	0.638
H10	4.282	1.165	4.681	0.194	3.942	0.149
H11	4.804	0.747	6.072	0.763	5.159	0.773
H12	4.410	1.000	5.087	0.047	4.506	0.087
H13	4.802	1.409	5.071	0.033	4.361	0.024
H14	4.179	1.148	5.038	0.017	4.337	0.011
H15	4.877	1.442	4.907	0.194	4.168	0.156
H16	5.430	0.513	7.055	0.150	6.003	0.133
H17	4.908	1.380	7.659	0.020	6.613	0.008
H18	4.147	1.334	6.812	0.266	5.950	0.218
H19	4.459	1.371	6.928	0.213	6.047	0.099
H20	5.076	1.102	6.944	0.166	5.800	0.144
H21	4.612	1.196	7.083	0.117	6.206	0.143
CH1	4.339	0.714	4.735	0.266	4.220	0.211
OH1	5.319	1.095	4.939	1.511	4.319	1.322
N1	3.952	1.009	4.247	0.038	3.672	0.026
N1H			3.263	0.043	2.825	0.032
N2	4.688	0.048	6.150	0.029	5.310	0.019
N2H					5.859	0.127

[a] Mean FPIX Fe−drug H distances (in angstroms) for complexes formed with neutral, +1, and +2 QN. These values are the initial distances from NMR T_1 experiments, followed by XPLOR refinement as described. The final values from all valid XPLOR output solutions were averaged to compute the mean, which is within 1 Å of the initial NMR experimental value for the +1 and +2 QN complexes and within 1.5 Å for the neutral QN complex.

Table 3: Quinidine−Fe Distances[a]

	neutral		monoprotic (+1)		diprotic (+2)	
atom	±1.50 Å	SD	±1.00 Å	SD	±1.00 Å	SD
H1	5.024	0.012	7.118	0.485	7.163	0.544
H2	4.922	0.025	6.727	0.363	6.839	0.181
H3	4.974	0.018	6.426	0.491	6.414	0.509
H4	5.072	0.010	6.341	0.502	6.329	0.415
H5	4.720	0.028	5.378	0.832	5.443	0.797
H6	5.100	0.111	6.177	0.993	6.568	0.707
H7	4.774	0.055	5.336	1.069	5.402	1.076
H8	4.607	0.019	6.434	1.028	6.853	0.956
H9	4.608	0.019	6.793	0.971	6.559	0.986
H10	3.605	1.577	6.919	0.741	7.178	0.065
H11	4.293	0.711	6.493	0.644	6.544	0.657
H12	4.143	0.605	5.942	1.037	5.962	1.090
H13	4.197	1.613	6.473	1.194	6.576	1.230
H14	4.151	1.200	7.211	1.051	6.991	1.191
H15	4.580	0.836	7.304	0.874	7.325	0.875
H16	3.334	0.674	6.421	0.873	6.461	0.842
H17	2.659	1.400	5.027	0.161	4.983	0.105
H18	3.375	1.536	5.706	0.796	5.667	0.792
H19	3.325	0.859	6.272	1.003	6.186	1.058
H20	3.152	0.760	6.540	0.787	6.495	0.750
H21	3.303	1.412	5.401	0.751	5.471	0.780
CH1	4.702	0.172	5.927	0.757	6.066	0.550
OH1	5.689	0.532	6.511	1.716	6.345	1.600
N1	3.818	0.877	6.546	0.264	6.602	0.227
N1H			7.287	0.323	7.361	0.274
N2	4.601	0.043	6.213	0.385	6.244	0.458
N2H					6.699	0.606

[a] Mean FPIX Fe−drug H distances (in angstroms) for complexes formed with neutral, +1, and +2 QD. These values are the initial distances from NMR T_1 experiments, followed by XPLOR refinement as described. The final values from all valid XPLOR output solutions were averaged to compute the mean, which is within 1 Å of the initial NMR experimental value for the +1 and +2 QD complexes and within 1.5 Å for the neutral QD complex.

aqueous solution at physiological DV pH (lower energy indicates a more stable complex). Although the affinity for the target is only one factor in determining clinical efficacy, this is interesting since Karle and co-workers previously showed a lower IC_{50} for QD than for QN (*26*). Although absolute energies differ, overall trends in binding energies for neutral versus monoprotic versus diprotic QN and QD are similar, with the neutral species of each being similarly less stable than either protonated species, as would be expected (*22*).

Closer inspection of the most stable (lowest-energy) QD versus QN solutions shows a subtle (but perhaps significant) difference for QD versus QN. Among the five or six lowest-energy structures (independent of the degree of basicity), the number of QD diprotic solutions is greater than the number of QD monoprotic solutions, whereas for QN, they are the same. That is, among drug−heme complexes that best satisfy the NMR distance constraints and that also have the lowest energies (<600 kcal/mol, indicating the most stable complexes possible), there are twice as many QD diprotic solutions as monoprotic, but an identical number of solutions for mono- and diprotic QN. This could be a coincidence related only to flexibility in the computer algorithm, but the result was obtained multiple times in multiple applications of XPLOR (not shown). If this does indeed imply a subtle pharmacological difference between QD and QN, it implies that protonation of the quinolinal N in QD provides slightly more stabilization for the complex relative to QN, resulting in lower energies and higher relative affinity for μ-oxo dimer as the pH is decreased toward the pK_a of the quinolinal N. The interesting implications are entertained in the Discussion.

Along with the trends in binding energies for QN versus QD, the plot for CQ shows additional interesting features. Namely, overall, binding of the neutral CQ complex appears to be more stable than binding of +1 or +2 CQ, which is the converse of the trend seen for QN and QD. Also, among lowest-energy solutions (<500 kcal/mol), there are approximately 3 times as many monoprotic CQ solutions as diprotic, which is the opposite of the trend seen for QN. Thus, even though the dibasic character of CQ is extremely important for concentrating the drug in the acid DV environment (*27*), it is not necessarily important for high-affinity binding to μ-oxo dimer FPIX. Investigation of the atomic level details of these structures helps to explain these trends.

Atomic Level Geometries of the Complexes. Figure 5 shows axial (top down) and side views of representative lowest-energy structures (<500 kcal/mol) for complexes formed between neutral (left), +1 (middle), and +2 (right) CQ and μ-oxo dimer FPIX. In these images, we fix the position of the aminoquinoline aromatic rings and allow all other atoms to position themselves accordingly. Superpositioning several of the lowest-energy structures from the XPLOR set of solutions (again, these are also the solutions most compatible with the Fe−H distances generated by the NMR experiments) provides an opportunity to view which features of the solution complex are "flexible" or relatively free to change orientation, and which are common to all of the low-energy structures and hence the most relevant with

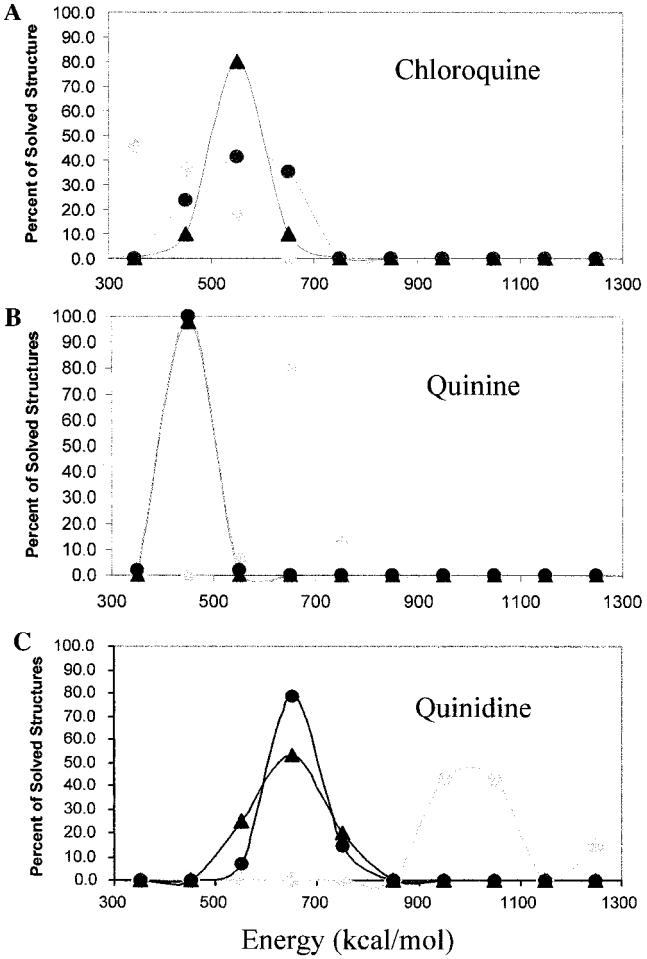

FIGURE 4: Plot of the energies for determined complexes between FPIX μ-oxo dimer and CQ (a) QN (b), and QD (c). In each panel, energies for complexes formed with neutral (◆), monoprotic (+1) (●), and diprotic (+2) (▲) drug are shown.

regard to in vivo pharmacology. Although in the case of CQ only the +2 CQ complex is physiologically relevant, comparing the three structures allows us to view the relative importance of protonation at N1 and N2 in stabilizing the physiologically relevant complex. In these images, the second FPIX tetrapyrrole in the dimer is omitted for clarity; it is attached to the FPIX complexed with drug via a nearly linear Fe−O−Fe bond. There is a hydroxyl ligand coordinated to the Fe on the opposite μ-oxo dimer face. In the presence of aminoquinoline drugs at the drug:FPIX ratios used in our experiments, each face of the dimer is in rapid equilibrium between covalent association with OH and noncovalent association with drug.

First, similar to earlier line broadening studies (*6*, *7*), our data are inconsistent with any covalent association between these aminoquinoline drugs and FPIX. Even though the quinolinal nitrogen (N2; cf. Figure 1) is predicted to be an excellent axial ligand for FPIX Fe, in the μ-oxo dimer the Fe is pulled in toward the bridging O (not shown). This makes the Fe unavailable for any Fe−N covalent bond. Conversely, monomeric FPIX and (for example) pyridine mixed together in organic solvents do indeed form covalent complexes (not shown). We note that such a covalent complex is certainly possible if the lifetime of FPIX monomers is long in the DV for any (currently undefined) reason; however, on the basis of current available information, the FPIX μ-oxo dimer likely dominates in the water-based environment of the DV.

Second, the axial views of the CQ complexes show the CQ aromatic rings positioned not over the FPIX Fe but more toward the edge of the FPIX tetrapyrrole. This is expected since it is where favorable $\pi-\pi$ electron interactions should be strongest. This positioning is unlike that hypothesized earlier for CQ, which put the center of the aromatic rings over the Fe center of FPIX (*6*, *7*), but it is similar to that suggested by Constantinidis and Sattlerlee for QN−uroheme noncovalent complexes (*9*). The axial view also shows that the positions of the FPIX side chains are essentially random relative to bound CQ for all three complexes. Note these positions are defined by XPLOR calculations that include explicit consideration of electrostatic energies; nonetheless, as described below, we do not find evidence for salt bridges between CQ $N1H^+$ and FPIX propionic acid COO^-. That is, relative to the fixed CQ aromatic rings, the tetrapyrrole monomer is free to spin like a "wheel" around an "axle" drawn from top to bottom through the Fe−O−Fe bond of the dimer, while the FPIX side chains wag up and down relative to the tetrapyrrole plane. This was initially puzzling to us since for the +1 CQ and +2 CQ complexes we, like others (*6*, *7*, *28*), expected favorable electrostatic interactions between the positively charged aliphatic N1 (cf. Figure 1) and the negatively charged propionic acid side chains of FPIX. The orientation of the CQ aliphatic side chain is in fact much less random than might be initially expected for such a flexible group, and it does not electrostatically interact with the FPIX side chains as initially predicted (*6*, *7*). Instead, it wraps back around, following the contour of the rim of the tetrapyrrole wheel. For the neutral complex, this feature is likely due to three factors, the first being an attraction between the lone pair of electrons on the aliphatic N and the positively charged Fe center and the second being van der Waals attractions between the heme plane and the CQ aliphatic chain. The third is a larger contribution that is obvious in hindsight and that also persists for the +1 and +2 CQ complexes, unlike the lone electron pair effect. This contribution is entropic in nature and is described in the Discussion.

The side views of these averaged structures highlight the interplanar distance between the drug and FPIX, as well as two angles of interest. For CQ, the anilinal N (N3; cf. the Figure 1 inset) to FPIX Fe distance decreases from a mean of ~3.4 Å, to 3.1 Å, to 2.8 Å for neutral, +1, and +2 drug, respectively, while the quinolinal N (N2) to Fe distance remains relatively constant. Hence there is a much higher degree of coplanarity for the lowest-energy +2 CQ complexes than for the neutral and +1 complexes (Figure 5, bottom), while the average interplanar distance remains similar. One angle of interest (α) is formed between the surface plane of FPIX and the long axis of the CQ aromatic rings (the long axis is drawn from the middle of the bond connecting carbons bonded to Cl and to H4 to the middle of the bond connecting carbons bonded to H1 and H5; cf. Figure 1), and the other angle (β) is formed between the FPIX face and the CQ aromatic short axis (drawn through the two carbons shared by the two rings of the quinoline moiety; see Figure 1). For the neutral CQ complex, α is nearly 0° whereas β is approximately 25° (Figure 5, bottom left). That is, "stacking" between the aromatic moieties of CQ and FPIX

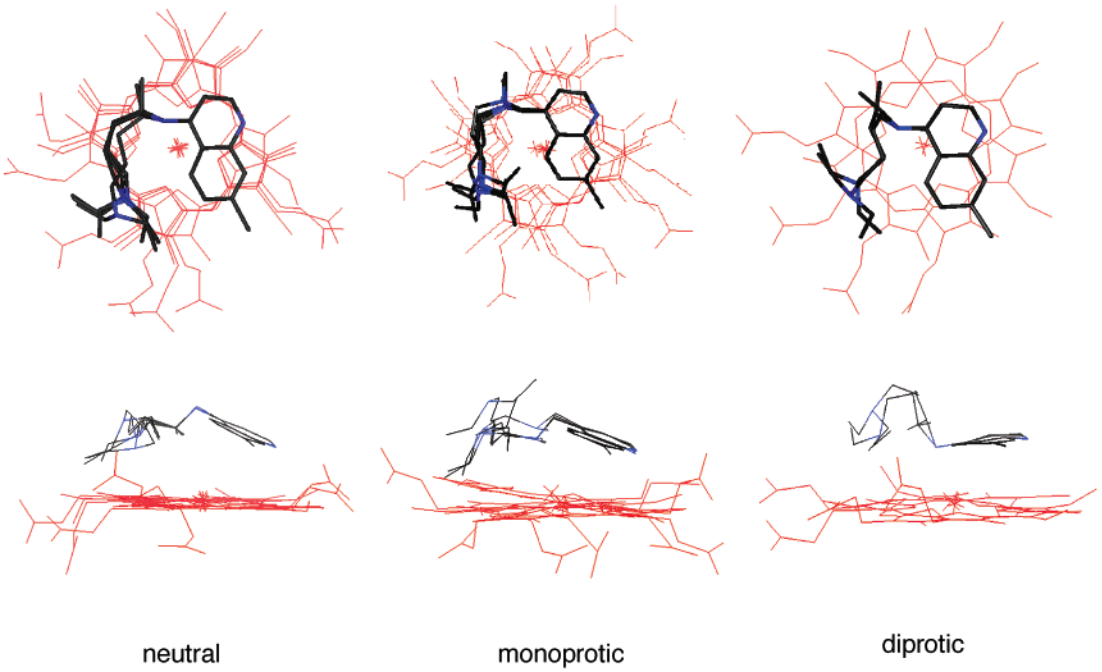

FIGURE 5: Axial (top) and side (bottom) views of superpositioned lowest-energy complexes formed between FPIX μ-oxo dimer and neutral (left), +1 (middle), and +2 (right) forms of CQ. Blue denotes N atoms on the drug, and red denotes the FPIX backbone. In these images, protons and the second FPIX monomer in the dimer are omitted for clarity. See the text for a detailed description.

(promoted by favorable interactions between π electrons) is not as coplanar as was previously proposed (*6*, *7*). In fact, there appears to be a slight tilt away from the Fe center. This also appears to be the case for the +1 CQ complex (Figure 5, bottom middle) and all of the QN and QD structures, where either α, β, or both are always >0° (see below). Simplistically, the degree of coplanarity might be predicted to be a rough measure of affinity, meaning the closer α and β are to 0°, the more stable the complex should be, since $\pi-\pi$ interactions between the aromatic rings would (simplistically) be predicted to be more favorable. However, comparing Figure 5 to Figure 4 shows that this simplistic scenario is incorrect; in fact, the neutral CQ species tends to form more lower-energy (higher-affinity) complexes relative to the diprotic species, but α and β are large for the low-energy neutral CQ complexes and nearly 0° for low-energy +2 CQ complexes (compare bottom left to bottom right of Figure 5). Thus, the energy of the complexes is determined by more than $\pi-\pi$ interactions. We suggest there is a significant van der Waals interaction between the oriented aliphatic side chain and the tetrapyrrole that is larger than initially anticipated (*6*).

When CQ is titrated from neutral to monobasic (+1), the distance between FPIX Fe and N1 increases from 4.7 to 5.3 Å presumably to keep the N1H positive charge a more comfortable distance away from the positive Fe (Table 1). When N2 is protonated to produce +2 CQ, α and β become nearly 0° (Figure 5, bottom right), surprisingly, N1 moves back to 4.6 Å from the FPIX Fe (Table 1), and the distance between FPIX Fe and N2 does not increase at all (Table 1). This appears to be somewhat paradoxical, since we expect the N2H and FPIX Fe also to be electrostatically repelled, and hence a trend similar to that observed upon initial titration of N1. We suggest that a balance among four terms explains this behavior, namely, (1) favorable $\pi-\pi$ electron overlap, (2) the favorable nature of the aliphatic chain wrapped back around the rim of the tetrapyrrole wheel (see the Discussion), (3) repulsion between FPIX Fe and N1H, and (4) repulsion between FPIX Fe and N2H. That is, in the CQ +2 complex, the two titratable protons are placed approximately equidistant from the Fe (Table 1) to minimize the sum of both unfavorable electrostatic interactions while preserving as much of the beneficial entropic (see the Discussion) and $\pi-\pi$ features that act to stabilize the complex. This scheme is consistent with the trend in energies shown in Figure 4a.

Figures 6 and 7 show similar panels that summarize the structures [again, neutral (left), +1 (middle), and +2 (right)] for QN and QD, respectively. Relative to CQ, there are four important differences. First, because the pK_a(2) values for QN and QD are close to DV pH estimates for CQR malaria (*10*), changes between +1 and +2 QN and QD complexes correspond to predicted in vivo pharmacology. Second, interplanar distances increase by 1−2 Å for these complexes relative to those for CQ. Third, the flexible CQ aliphatic side chain is replaced with a much less flexible bridged cyclic side chain in QN and QD, and fourth, the aniline N in CQ (N3; cf. Figure 1) is replaced with an alcohol that will carry a small positive dipole moment pointed away from the O toward the alcohol H (Figure 1). Moreover, the OH group is attached to one of the two chiral centers that distinguish QN from QD (Figure 1), and since the quinolinal rings are once again positioned more to the periphery of the tetrapyrrole, the OH is conspicuously superpositioned over FPIX Fe. Thus, not coincidentally, a review of the lowest-energy structures implies that for the QN structures, this OH group is typically pointed away from FPIX Fe (to presumably minimize repulsion between FPIX Fe and the positive end of the OH dipole) while compromising α or β relatively little [0° > α > 10° (Figure 6, left to right), β < 10° (Figure 6, left to middle)], to maximize favorable $\pi-\pi$ interactions. β does increase dramatically to approximately 35° for neutral

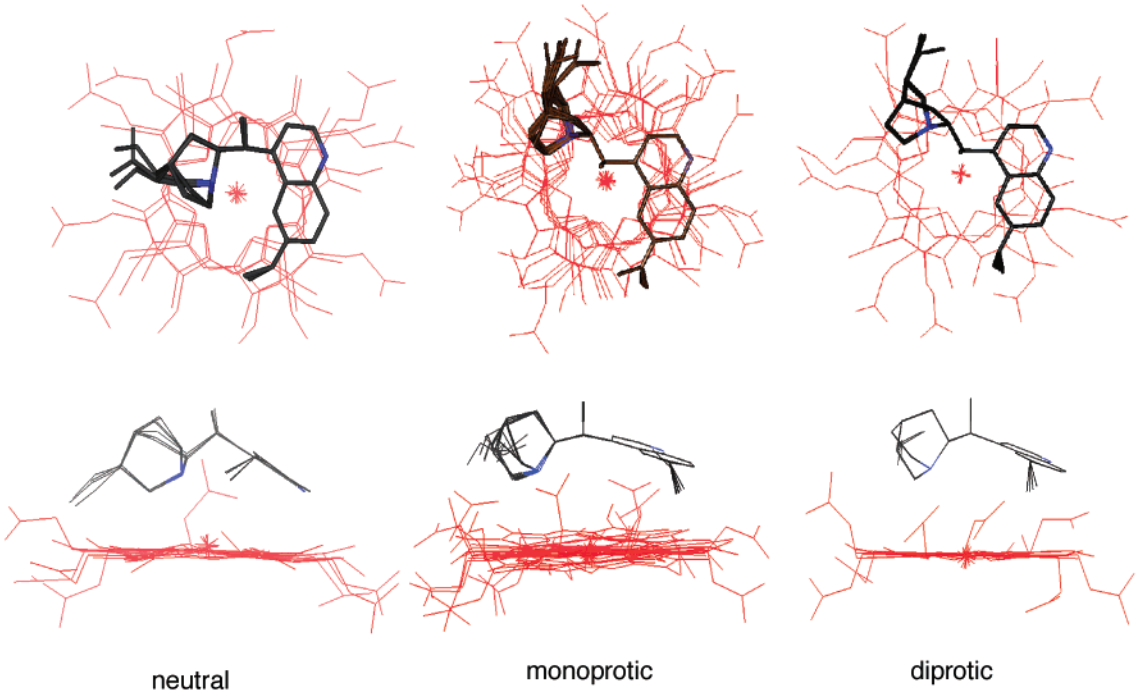

FIGURE 6: Axial (top) and side (bottom) views of superpositioned lowest-energy complexes formed between FPIX μ-oxo dimer and neutral (left), +1 (middle), and +2 (right) forms of QN. Blue denotes N atoms on the drug, and red denotes the FPIX backbone. In these images, protons and the second FPIX monomer in the dimer are omitted for clarity. See the text for a detailed description.

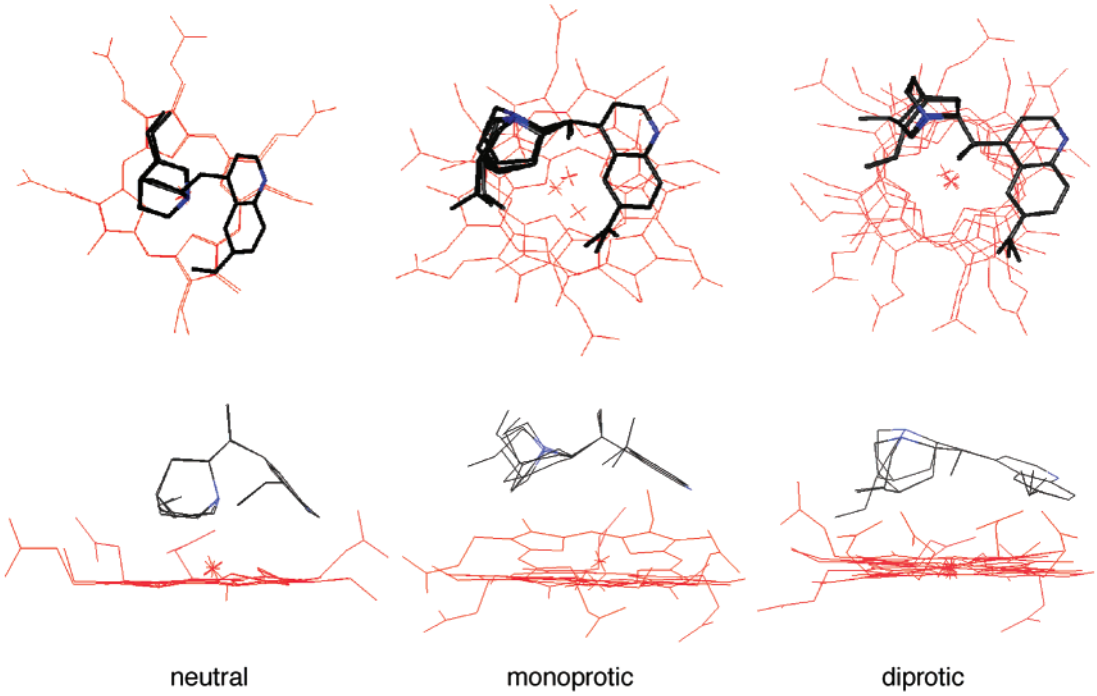

FIGURE 7: Axial (top) and side (bottom) views of superpositioned lowest-energy complexes formed between FPIX μ-oxo dimer and neutral (left), +1 (middle), and +2 (right) forms of QD. Blue denotes N atoms on the drug, and red denotes the FPIX backbone. In these images, protons and the second FPIX monomer in the dimer are omitted for clarity. See the text for a detailed description.

QN bound to FPIX (Figure 6, left), which likely contributes strongly to the higher energy (lower affinity) for this nonphysiological complex (cf. Figure 4). In contrast, because of the stereochemistry at C1 (cf. Figure 1) and the relative inflexibility of the side chain which is (similar to CQ) compelled to establish favorable van der Waals contacts, QD is forced to compromise α or β more dramatically for the physiologically relevant +1 and +2 QD structures to properly position the OH group. This effect is most dramatic in the middle and right panels of Figure 7 where α and β are approximately 50° and 10° (middle) and 25° and 20° (right), respectively. Again, this result initially appears to be paradoxical since Karle and colleagues previously measured a lower IC_{50} for QD than for QN for both drug sensitive and drug resistant malarial parasites (*26*). The paradox is addressed in the Discussion.

Finally, the pattern for N1 (aliphatic) and N2 (quinolinal; see Figure 1) to FPIX Fe distances upon protonation (neutral

to +1 to +2) is again interesting. For QN N1, the pattern (3.95 Å to 4.25 Å to 3.67 Å, respectively) qualitatively mirrors the surprising pattern for CQ, whereas in the QD +2 complex, QD N1 manages to remain outside a distance that would feel repulsion from FPIX Fe. However, since +2 CQ and +2 QN form higher-affinity complexes than +2 QD, again, the predicted repulsion between $N1H^+$ and FPIX Fe does not negatively impact the stability of the complexes as much as might be initially suspected. Both QN and QD manage to position N2 far from FPIX Fe upon protonation of the group as would be predicted, but this could be fortuitous since N2 is already distant in the +1 complex for both QN and QD.

DISCUSSION

This paper presents the first atomic level structures for solution complexes formed between several important antimalarials and the FPIX μ-oxo dimer. We note that soluble μ-oxo dimer FPIX may not be the only heme-derived antimalarial drug target (*12*). This species is dominant in routine aqueous laboratory solutions, but the DV environment aggregates the μ-oxo dimer and converts FPIX to the Fe−O41 dimer that forms the unit cell of hemozoin (*1*). The relative abundance of μ-oxo versus Fe−O41 dimers, soluble versus aggregated (but not crystalline) forms of these (*27*), and even of dimer versus (presumably short-lived) monomer FPIX is presently unclear. Understanding how these drugs bind to and influence physiologic equilibria between these forms is vital (*29*), and this paper represents only the first step in that regard.

Historically, the through space effect of paramagnetic centers on H resonances has been a useful NMR technique with several applications (*30*). Since FPIX has a paramagnetic Fe center, paramagnetic effects on drug H resonances could in theory be used to precisely map drug−heme complex geometries. In this study, we show such an analysis is indeed possible by combining longitudinal relaxation experiments with energy minimization. This paper significantly refines the structures of antimalarial drug−FPIX dimer complexes. Previous work (*7*) suggested a FPIX dimer−CQ complex structure based on broadening of CQ proton resonances upon addition of heme. The extent of broadening of peaks corresponding to aromatic protons was greater than that for aliphatic protons, so as a result of the effects being ranked, a likely "coplanar" geometry was suggested with an estimated interplanar distance between 3 and 5 Å (*7*). However, precise atomic distances were not determined, and heme side chain orientation was not elucidated. The picture that emerged from these early studies is similar to the structures we now report, but there are several important differences. Namely, the degree of coplanarity (parallel orientation of drug aromatic vs tetrapyrrole rings) in these early structures was somewhat overestimated, and the aromatic rings were placed too close to the Fe center of the tetrapyrrole when in fact they are positioned much closer to the edge.

Atomic level definition of heme and drug side chain positions is actually quite important, since modification of heme side chains is an intricate step in hemozoin formation, and side chain modifications of CQ have important effects on activity (*31*). The nonrandom orientation of aliphatic drug side chains that we find is quite interesting. If the flexible +1 or +2 CQ side chain extended out past the rim of the FPIX wheel (as we and others initially guessed) to complex $N1H^+$ to a propionic acid FPIX side chain, it would prevent free rotation of one FPIX tetrapyrrole versus its partner in the dimer. Free rotation should occur along the Fe−O−Fe bond. Extending the aliphatic side chain past the rim of the wheel would also hinder "up and down" free movement of the FPIX side chains (Figure 5). The point is, the high entropic "cost" in such a restrictive scenario presumably outweighs the enthalpic "benefit" from a CQ $N1H^+$−FPIX COO^- salt bridge.

Exploring the implications of this CQ side chain orientation may assist interpretation of ongoing structure−function analysis of antimalarial drugs (*31*). From the axial images presented in this paper (Figure 5, top), we can see that lengthening the chain more than three carbons would force the end of the CQ aliphatic chain outside the rim of the FPIX wheel, and/or very near the aminoquinolinal ring. Conversely, shortening the aliphatic chain would lower the stabilizing van der Waals contribution, but would also allow for structures with variable CQ N1H− and N2H−FPIX Fe distances. Exploring arguments such as these in the context of emerging data on the physiology of the DV for CQR parasites (*10*, *27*) should provide additional insight into the activity of various quinolines. Overall, if the availability of the free FPIX dimer is indeed reduced for CQR parasites as is predicted from recent DV pH measurements (*10*, *13*, *14*), then *all* (of at least four) factors that contribute to formation of the most stable CQ−FPIX dimer complexes become even more vital. Additional concepts will likely become apparent upon examining structures of complexes formed by CQ analogues.

Changes in DV pH have been measured for CQR parasites (*10*), and consideration of how these could affect overall binding for a DV drug *population* is also important. For example, another interesting result is that the mean energy of the lowest-energy structures for diprotic QD is slightly lower than that for monoprotic QD, whereas these two are nearly identical for QN. Also, despite lower in vivo IC_{50} values for QD than for QN (*26*), QN forms a lower-energy (more stable) complex relative to QD, regardless of whether they are neutral, +1, or +2. With regard to this apparent paradox, "bioavailability" is at least as relevant as target affinity. Although they are isomers, QN and QD actually differ in quinolinal N pK_a, with that of QD being 0.2−0.3 higher (L. M. B. Ursos and P. D. Roepe, unpublished results). Some fraction of QD and QN indeed exists in diprotic form within the DV (∼20−30%). For CQS parasites with a DV pH near 5.5 (*10*), the percent diprotic will be lower and similar for QN and QD. However, at a lower DV pH (5.0−5.2) suggested for CQR parasites (*10*, *13*), the dibasic species can rise to more than 30% of total DV-associated drug, and +2 QD will be ∼2-fold higher than +2 QN, because accumulation of the monoprotic drug within acidic compartments depends linearly on the net ΔpH whereas accumulation of the diprotic drug depends on the square of ΔpH (*27*). Even though diprotic species are a smaller component of the overall QN or QD drug population in the DV, at an appropriate DV pH QD is predicted to have higher bioavailability (more QD than QN at the site of action). Moreover, since among the lowest-energy solutions there are at least

twice as many diprotic QD structures as monoprotic structures, but equal numbers of di- and monoprotic QN solutions, in a low-pH environment, relative binding of QD populations should improve as the pH is lowered, while that of QN stays the same. That is, since the energy of +2 QN complexes is the same as that of +1 complexes, there would be no overall increase in the affinity of +1 QN/+2 QN mixtures as the pH is lowered, but there is predicted to be an increase for QD.

This last point is particularly interesting, since Cooper et al. have recently showed that as the DV pH is lowered in 76I *pfcrt* mutants (*32*), they acquire CQ and QD resistance but become hypersensitive to QN. The relevant DV pH measurements were taken in the absence of QN and QD, so there may be additional phenomena to uncover for this important mutant. Nonetheless, assuming μ-oxo dimer is the primary drug target, we could easily rationalize a hypersensitivity to QD via the above arguments. In contrast, a lower DV pH alone (in the absence of any effect on the DV pH by these drugs) does not easily explain QN hypersensitivity in the 76I mutant, unless QN binds to solid state (aggregated) heme better than QD and CQ do.

Additional NMR studies will be required to determine distance constraints for drug−FPIX complexes formed in the solid state. However, since there appears to be free rotation of heme around the Fe−O−Fe axis and no obvious electrostatic pairing between the NH^+ group on drug side chains and the COO^- group on FPIX side chains, ionic interactions between μ-oxo FPIX and drug side chains may play only a small role in stabilizing solid state complexes. Complexes that might form with Fe−O41 dimers, wherein rotation of the wheel will be altered (*1*), are more difficult to predict and hence the most enticing yet to explore.

ACKNOWLEDGMENT

We thank our colleague R. Bachmann for helpful discussions and M. McMahon for the heme force field used in our initial calculations. We also thank the Department of Chemistry at the University of Illinois at Chicago for generously providing computer time for this project.

SUPPORTING INFORMATION AVAILABLE

Graph of the relationship between the effective magnetic moment and the CQ:HT ratio. This material is available free of charge via the Internet at http://pubs.acs.org.

REFERENCES

1. Pagola, S., Stephens, P. W., Bohle, D. S., Kosar, A. D., and Madsen, S. K. (2000) *Nature 404*, 307−310.
2. Slater, A. F., and Cerami, A. (1992) *Nature 355*, 167−169.
3. Dorn, A., Stoffel, R., Matile, H., Bubendorf, A., and Ridley, R. G. (1995) *Nature 374*, 269−271.
4. Munro, O. Q., Madlala, P. S., Warby, R. A. F., Seda, T. B., and Hearne, G. (1999) *Inorg. Chem. 38*, 4724−4736.
5. Ellison, M. K., and Scheidt, W. R. (1999) *J. Am. Chem. Soc. 121*, 5210−5219.
6. Moreau, S., Perly, B., and Biguet, J. (1982) *Biochimie 64*, 1015−1025.
7. Moreau, S., Perly, B., Chachaty, C., and Deleuze, C. (1985) *Biochim. Biophys. Acta 840*, 107−116.
8. Constantinidis, I., and Satterlee, J. D. (1988) *J. Am. Chem. Soc. 110*, 927−932.
9. Constantinidis, I., and Satterlee, J. D. (1988) *J. Am. Chem. Soc. 110*, 4391−4395.
10. Dzekunov, S. M., Ursos, L. M. B., and Roepe, P. D. (2000) *Mol. Biochem. Parasitol. 110* (1), 107−124.
11. Ursos, L. M. B., Dzekunov, S. M., and Roepe, P. D. (2000) *Mol. Biochem. Parasitol. 110* (1), 125−134.
12. Ursos, L. M. B., DuBay, K. F., and Roepe, P. D. (2001) *Mol. Biochem. Parasitol. 112* (1), 11−17.
13. Fidock, D. A., Nomura, T., Talley, A. K., Cooper, R. A., Dzekunov, S. M., Ferdig, M. T., Ursos, L. M. B., Sidhu, A. B., Naude, B., Deitsch, K. W., Su, X. Z., Wootton, J. C., Roepe, P. D., and Wellems, T. E. (2000) *Mol. Cell 6* (4), 861−871.
14. Mehlotra, R. K., Fujioka, H., Roepe, P. D., Janneh, O., Ursos, L. M. B., Jacobs-Lorena, V., McNamara, D. T., Bockarie, M. J., Kazura, J. W., Kyle, D. E., Fidock, D. A., and Zimmerman, P. A. (2001) *Proc. Natl. Acad. Sci. U.S.A. 98* (22), 12689−12694.
15. Martiney, J. A., Ferrer, A. S., Cerami, A., Dzekunov, S., and Roepe, P. D. (1999) Transport and Trafficking in the Malaria Infected Erythrocyte, *Novartis Found. Symp. 226*, 265−281.
16. Poli-Scaife, S., Attias, R., Dansette, P. M., and Mansuy, D. (1997) *Biochemistry 36*, 12672−12682.
17. Dorn, A., Vippagunta, S. R., Matile, H., Jaquet, C., Vennerstrom, J. L., and Ridley, R. G. (1998) *Biochem. Pharmacol. 55* (6), 727−736.
18. Evans, D. F. (1959) *J. Chem. Soc.*, 2003−2005.
19. Grant, D. H. (1995) *J. Chem. Educ. 72* (1), 39−40.
20. Modi, S., Primrose, W. U., Boyle, J. M. B., Gibson, C. F., Lian, L. Y., and Roberts, G. C. K. (1995) *Biochemistry 34*, 8982−8988.
21. Dijkstra, G. D. H., Kellogg, R. M., Wynberg, H., Svendsen, J. S., Marko, I., and Sharpless, K. B. (1989) *J. Am. Chem. Soc. 111* (21), 8069−8076.
22. Egan, T. J., Hunter, R., Kaschula, C. H., Marques, H. M., Misplon, A., and Walden, J. (2000) *J. Med. Chem. 43*, 283−291.
23. Nilges, M., Clore, G. M., and Gronenborn, A. M. (1988) *FEBS Lett. 229*, 317−324.
24. Nilges, M., Kuszewski, J., and Brunger, A. T. (1991) in *Computational Aspects of the Study of Biological Macromolecules by NMR* (Hoch, J. C., Ed.) Plenum Press, New York.
25. Kuszewski, J., Nilges, M., and Brunger, A. T. (1992) *J. Biomol. NMR 2*, 33−56.
26. Karle, J. M., and Bhattacharjee, A. K. (1999) *Bioorg. Med. Chem. 7*, 1769−1774.
27. Ursos, L. M. B., and Roepe, P. D. (2002) *Med. Res. Rev.* (in press).
28. O'Neill, P. M., Willock, D. J., Hawley, S. R., Bray, P. G., Storr, R. C., Ward, S. R., and Park, B. K. (1997) *J. Med. Chem. 40*, 437−448.
29. Chou, A. C., Chevli, R., and Fitch, C. D. (1980) *Biochemistry 19*, 1543−1549.
30. La Mar, G. N., Horrocks, W. deW., Jr., and Holm, R. H. (1973) *NMR of Paramagnetic Molecules, Principles and Applications*, Academic Press, New York.
31. De, D., Krogstad, F. M., Byers, L. D., and Krogstad, D. J. (1998) *J. Med. Chem. 41* (25), 4918−4926.
32. Cooper, R. A., Ferdig, M. T., Su, X.-z., Ursos, L. M. B., Mu, J., Nomura, T., Fujioka, H., Fidock, D. A., Roepe, P. D., and Wellems, T. E. (2002) *Mol. Pharmacol. 61*, 1−8.

BI020195I